Available online at www.sciencedirect.com

ScienceDirect

IFAC PapersOnLine 54-20 (2021) 134–140

Robust control of rotation-floating space robots with flexible appendages for on-orbit servicing

Sofiane Kraïem * **Mathieu Rognant** ** **Jean-Marc Biannic** **
Yves Brière *

* *ISAE-SUPAERO, Université de Toulouse, France (e-mail: sofiane.kraiem@isae-supaero.fr).*
** *ONERA, Toulouse, France*

Abstract: On-orbit operations are facing a growing need for autonomous robotic systems to achieve risky and repetitive tasks. Debris removal, on-orbit servicing and in-space deployment/assembly are examples of applications considering the use of robot manipulators. The presence of large and light appendages in future spacecrafts, such as solar arrays, antennas and sun shields yields to flexible disturbances inside the structure making the control of the manipulator challenging. This paper addresses design and control problems related to autonomous space manipulator system when using kinetic moment exchange devices in presence of systems disturbances and model uncertainties. A common control of the manipulator and the base spacecraft is introduced for a free-floating space manipulator. An Extended State Observer (ESO) is developed to obtain the Nonlinear Dynamic Inversion (NDI) and improve manipulator control performances. A simultaneous synthesis of a control law gain and observer gain is proposed with a Linear Matrix Inequalities (LMI) resolution to tackle system variations and uncertainties. Illustration of the proposed method's efficiency and feasibility is obtained with simulations run on an actual space telescope assembly.

Keywords: Space manipulator, Extended State Observer, Nonlinear Dynamic Inversion, Disturbance Compensation

1. INTRODUCTION

The near-future of space missions is writing itself with space robots which are expected to play a first role in the mission's success. Risky and highly repetitive tasks are fostering less the use of various robotic systems to the detriment of manned missions (see Flores-Abad et al. (2014)). Yet, for in-space capture, deployment and on-orbit servicing operations, robotic systems will require to become autonomous to be a viable solution (see Li et al. (2019b)).

In the wild range of On-Orbit Servicing (OOS) applications, on-orbit deployment has developed an increasing interest for the use of space manipulators and likewise allows to illustrate the problematics common to maintenance operations and capture of failing satellites. One can depict the future of spacecrafts as large structures with light appendages too large to be self-deployed or requiring in-space assembly with cooperative modular components as presented in Lu et al. (2020). Also the future of space telescopes allows to illustrate the necessity of new technologies for space manipulators as illustrated in Song et al. (2019) and specially the importance of autonomous control as explained in Rognant et al. (2019a).

One challenging and remaining task for space manipulators to become autonomous is achieving attitude control during manipulator motions as manipulator motions affect both linear and angular spacecraft dynamics. Studies have been made for capture applications as potentially tumbling targets require adapted manipulator approaches. Efficient use of thrusters to compensate manipulator motions have been studied through workspace adjustment strategies as proposed in Giordano et al. (2018), or simultaneous control of the global center of mass and spacecraft attitude in Giordano et al. (2019). Likewise, when only the manipulator is controlled, reaction null-space control has been developed in Pisculli et al. (2015) to reduce interactions between the manipulator and the spacecraft base. One can also note the cases when no base actuators are considered. More generally, trajectory planning are considered to reduce the impact of the manipulator motions and/or external disturbances on the base at least for singularity-free trajectories. A Nonlinear Model Predictive Control has been employed in Rybus et al. (2017) to ensure manipulator realization of an optimized trajectory that minimizes manipulator disturbances on the satellite, likewise during capture approach phase a Cartesian trajectory planning has been studied in Lu and Yang (2020) to minimize attitude disturbances, a common trajectory planning for collision-free path and singularity-free path for fuel consumption optimizations is proposed in Seddaoui and Saaj (2019) while the internal and external perturbations are tackled with $\mathbf{H}_\infty$ control and feedforward compensations.

Moreover, future spacecrafts will be expecting longer lifespan with the use of electrical kinetic moment exchange

10.1016/j.ifacol.2021.11.165

devices instead of thrusters to control the base attitude, such space manipulators are defined in Wilde et al. (2018) as rotation free-floating. During OOS missions, relatively high mass and inertia are considered which is why the use of kinetic moment exchange devices has raised an interest to deal with the momentum in the system created by the manipulator on the base as proposed in Li et al. (2013). Kinetic indices have allowed to highlight the advantages to simultaneously control the manipulator and the base actuators to increase manipulator's manipulability as detailed in Rognant et al. (2019b). Likewise combining reaction wheels and control moment gyroscopes has been studied in Wu et al. (2018) to maintain the satellite platform fixed during manipulator motions.

The manipulator motions create vibrations of the flexible appendages due to the coupled flexible dynamics of the base and the rigid dynamics of the manipulator. Control based on factors evaluating the coupling between rigid and flexible dynamics have been developed in Meng et al. (2018) to suppress the vibrations due to manipulator motions. Coupling factors can as well be used to optimize the manipulator trajectories that minimize base disturbances as suggested in Li et al. (2019a). In order to improve manipulator control performances, a disturbance observer has been developed in Wu et al. (2018) with a vibration active control to reduce the manipulator perturbations. With rigid spacecraft hypothesis, unknown disturbances observer and robust control have been proposed in Qiao et al. (2019). In Kraïem et al. (2021), by deriving the rigid-flexible dynamics of a rotation free-floating space manipulator, a disturbance observer allows to include disturbances in the system linearization to adapt perturbation rejection and improve manipulator control performances.

As an extension of our previous work Kraïem et al. (2021), this paper aims at developing the common control of the spacecraft base and manipulator under structural disturbances and system uncertainties thanks to an ESO. Novelties in this paper are: the development of the ESO generalized to a larger set of OOS applications, the simultaneous synthesis of observer and controller gains that includes measurement errors and uncertainties on the system parameters, and the consideration of the system inertia variations through the space manipulator motions

The paper is organised as follows, firstly the dynamics of a rotation free-floating spacecraft with a rigid manipulator and flexible appendages are detailed, secondly a common control of the manipulator and the spacecraft base attitude is developed and thirdly the proposed method efficiency is illustrated on an on-orbit telescope deployment.

2. SYSTEM OPEN-LOOP DYNAMICS REDUCTION

2.1 Problem statement

In this study we consider a rotation free-floating spacecraft equipped with a serial-link manipulator with n_q degrees of freedom and whose base attitude is controlled by n_r reaction wheels. The manipulator joints are either prismatic or revolute joints. Solar arrays and sun shields connected to the satellite base present flexible dynamics. Moreover, the linear dynamics of the spacecraft and the flexible dynamics are not measurable, only actuators velocities and poses as well as base attitude dynamics are available. In this study, neither environmental nor external forces are considered here and no initial momentum hypotheses are made.

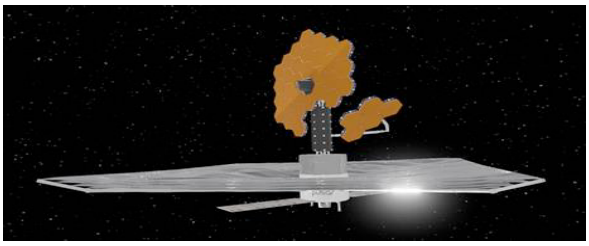

Fig. 1. Illustration of the studied spacecraft (Rognant et al. (2019a))

2.2 Dynamics of a rigid space manipulator with flexible appendages

The dynamics of a rigid multi-body system with no external forces applied to it, can be expressed as in Rognant et al. (2019b):

$$\underbrace{\begin{bmatrix}\mathbf{H}_0 & \mathbf{H}_{0q}\\ \mathbf{H}_{0q}^T & \mathbf{H}_q\end{bmatrix}}_{\mathbf{H}(\mathbf{q})}\begin{bmatrix}\dot{\boldsymbol{\omega}}_0\\ \ddot{\mathbf{p}}_0\\ \ddot{\mathbf{q}}\end{bmatrix}+\underbrace{\begin{bmatrix}\mathbf{C}_0 & \mathbf{C}_{0q}\\ \mathbf{C}_{0q}^T & \mathbf{C}_q\end{bmatrix}}_{\mathbf{C}(\mathbf{q},\dot{\mathbf{q}},\boldsymbol{\omega}_0,\dot{\mathbf{p}}_0)}\begin{bmatrix}\boldsymbol{\omega}_0\\ \dot{\mathbf{p}}_0\\ \dot{\mathbf{q}}\end{bmatrix}=\begin{bmatrix}\mathbf{0}\\ \boldsymbol{\tau}_q\end{bmatrix} \quad (1)$$

where $\boldsymbol{\omega}_0 \in \mathbb{R}^{3\times 1}$ and $\dot{\mathbf{p}}_0 \in \mathbb{R}^{3\times 1}$ are respectively the base spacecraft angular and linear velocity vector, $\dot{\mathbf{q}} = \begin{bmatrix}\dot{\mathbf{q}}_r^T & \dot{\mathbf{q}}_m^T\end{bmatrix}^T \in \mathbb{R}^{n_q\times 1}$ (with $n_q = n_r + n_m$) is the reaction wheels and joint velocity vector and $\boldsymbol{\tau}_q = \begin{bmatrix}\boldsymbol{\tau}_r^T & \boldsymbol{\tau}_m^T\end{bmatrix}^T \in \mathbb{R}^{n_q\times 1}$ the actuator torques.

$\mathbf{H}$ is a nonlinear matrix dependent on the manipulator and spacecraft configuration, and is the symmetric, positive-definite generalized inertia matrix including both the inertia coupling matrices between the base and the manipulator, $\mathbf{H}_{0m}$, and between the base and the kinetic moment exchange devices, $\mathbf{H}_{0r}$. $\mathbf{C}$ is a nonlinear convective matrix dependent on the manipulator and spacecraft velocity and configuration.

Using the hybrid-Cantilvered model with the assumption of no external forces and torques applied to the system, the dynamics of a rigid-flexible multi-body are given by (see Kraïem et al. (2021)):

$$\begin{aligned}&\begin{bmatrix}\mathbf{H}_\omega & \mathbf{H}_{\omega L} & \mathbf{H}_{\omega q} & \mathbf{H}_{\omega\eta}\\ \mathbf{H}_{L\omega} & \mathbf{H}_L & \mathbf{H}_{Lq} & \mathbf{H}_{L\eta}\\ \mathbf{H}_{\omega q}^T & \mathbf{H}_{Lq}^T & \mathbf{H}_q & \mathbf{0}\\ \mathbf{H}_{\omega\eta}^T & \mathbf{H}_{L\eta}^T & \mathbf{0} & \mathbf{H}_\eta\end{bmatrix}\begin{bmatrix}\dot{\boldsymbol{\omega}}_0\\ \ddot{\mathbf{p}}_0\\ \ddot{\mathbf{q}}\\ \ddot{\boldsymbol{\eta}}\end{bmatrix}\\ &+\begin{bmatrix}\mathbf{C}_\omega & \mathbf{C}_{\omega L} & \mathbf{C}_{\omega q} & \mathbf{C}_{\omega\eta}\\ \mathbf{C}_{L\omega} & \mathbf{C}_L & \mathbf{C}_{Lq} & \mathbf{C}_{L\eta}\\ \mathbf{C}_{\omega q}^T & \mathbf{C}_{Lq}^T & \mathbf{C}_q & \mathbf{0}\\ \mathbf{C}_{\omega\eta}^T & \mathbf{C}_{L\eta}^T & \mathbf{0} & \mathbf{C}_\eta\end{bmatrix}\begin{bmatrix}\boldsymbol{\omega}_0\\ \dot{\mathbf{p}}_0\\ \dot{\mathbf{q}}\\ \dot{\boldsymbol{\eta}}\end{bmatrix}\\ &+\begin{bmatrix}\mathbf{0} & \mathbf{0} & \mathbf{0} & \mathbf{0}\\ \mathbf{0} & \mathbf{0} & \mathbf{0} & \mathbf{0}\\ \mathbf{0} & \mathbf{0} & \mathbf{0} & \mathbf{0}\\ \mathbf{0} & \mathbf{0} & \mathbf{0} & \mathbf{K}_\eta\end{bmatrix}\begin{bmatrix}\boldsymbol{\theta}_0\\ \mathbf{p}_0\\ \mathbf{q}\\ \boldsymbol{\eta}\end{bmatrix}=\begin{bmatrix}\mathbf{0}\\ \mathbf{0}\\ \boldsymbol{\tau}_q\\ \mathbf{0}\end{bmatrix}\end{aligned} \quad (2)$$

where η is the modal coordinate vector of the n_η flexible modes. The base angular and linear contribution of each

matrix on the base are decomposed using respectively subscripts $_\omega$ and $_L$.

2.3 Simulation tools

Numerical simulations are obtained with a Matlab-Simulink simulator based on the integration of the Satellite Dynamic Toolbox (see Alazard et al. (2008)) into the toolbox SPART (see Virgili-Llop et al. (no date)). The simulator allows to compute a rigid-flexible multi-body system: kinematics, differential kinematics, dynamics and forward/inverse dynamics. An XML description of the system, in which each parts are detailed, is required for numerical or symbolic analysis and simulations. Time-domain simulations are obtained with Simulink.

3. CONTROL STRATEGY

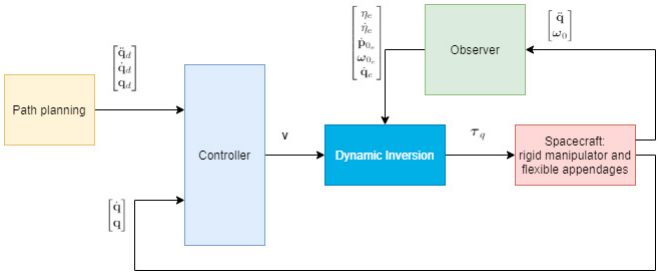

Fig. 2. Block diagram of the proposed control

A common manipulator and reaction wheels control is developed, as path planner methods provide manipulator trajectories and velocities as well as the velocities of reaction wheels. This is why a common manipulator and reaction wheels control is developed. Control performances are improved with the integration of internal disturbances in the feedback linearization that decouples actuators. A simultaneous observer and control gain synthesis is proposed while considering system variations and uncertainties as well as measurement errors.

3.1 Observer dynamics

In order to proceed to the feedback linearization, an estimation of the vibrations (i.e. $\dot{\boldsymbol{\eta}}, \boldsymbol{\eta}$) and the linear dynamics (i.e. $\dot{\mathbf{p}}_0$) is required. The observer is designed using available measurements of the manipulator actuators accelerations (i.e. $\ddot{\mathbf{q}}_m$) and reaction wheels accelerations (i.e. $\ddot{\mathbf{q}}_r$).

From (2), one can write the linear and angular dynamics of the spacecraft as well as the flexible dynamics such that (see appendix for details):

$$\begin{bmatrix} \ddot{\boldsymbol{\eta}} \\ \dot{\mathbf{p}}_0 \\ \dot{\boldsymbol{\omega}}_0 \end{bmatrix} = -\mathbf{M}^*(\mathbf{q})\ddot{\mathbf{q}} - \mathbf{D}^*(\mathbf{q}, \dot{\mathbf{q}}, \boldsymbol{\omega}_0, \dot{\mathbf{p}}_0) \begin{bmatrix} \dot{\boldsymbol{\eta}} \\ \dot{\mathbf{p}}_0 \\ \boldsymbol{\omega}_0 \\ \dot{\mathbf{q}} \end{bmatrix} - \mathbf{K}^*(\mathbf{q})\boldsymbol{\eta} \tag{3}$$

In order to estimate the drift of the spacecraft and the appendages flexible vibrations, one can introduce the state vector $\mathbf{x} = \left[\eta^T \ \dot{\eta}^T \ \dot{\mathbf{p}}_0^T \ \boldsymbol{\omega}_0^T \ \dot{\mathbf{q}}^T\right]^T$, the command vector $\mathbf{u} = \ddot{\mathbf{q}}^T$ and the output vector $\mathbf{y} = \left[\boldsymbol{\omega}_0^T \ \dot{\mathbf{q}}^T\right]^T$ and with (3) one can write:

$$\begin{cases} \dot{\mathbf{x}} = \begin{bmatrix} \mathbf{0} & [\mathbf{I}\ \mathbf{0}] \\ -\mathbf{K}^*(\mathbf{q}) & -\mathbf{D}^*(\mathbf{q}, \dot{\mathbf{q}}, \boldsymbol{\omega}_0, \dot{\mathbf{p}}_0) \\ \mathbf{0} & \mathbf{0} \end{bmatrix} \mathbf{x} \\ \quad + \begin{bmatrix} \mathbf{0} \\ -\mathbf{M}^*(\mathbf{q}) \\ \mathbf{I} \end{bmatrix} \mathbf{u} = \mathbf{A}_e(\mathbf{q}, \dot{\mathbf{q}}, \boldsymbol{\omega}_0, \dot{\mathbf{p}}_0)\mathbf{x} + \mathbf{B}_e(\mathbf{q})\mathbf{u} \end{cases} \tag{4a}$$

$$\mathbf{y} = \begin{bmatrix} \mathbf{0} & \mathbf{0} & \mathbf{0} & \mathbf{I} & \mathbf{0} \\ \mathbf{0} & \mathbf{0} & \mathbf{0} & \mathbf{0} & \mathbf{I} \end{bmatrix} \mathbf{x} = \mathbf{C}_e\mathbf{x} \tag{4b}$$

The state $\mathbf{x}$ is estimated as $\mathbf{x}_e$ through a linear observer of gain $\mathbf{L}$, with an LMI resolution as detailed in 3.4. The observer dynamic is given by:

$$\dot{\mathbf{x}}_e = \mathbf{A}_e(\mathbf{q}, \dot{\mathbf{q}}, \boldsymbol{\omega}_0, \dot{\mathbf{p}}_0)\mathbf{x}_e + \mathbf{B}_e(\mathbf{q})\mathbf{u} + \mathbf{L}(\mathbf{y} - \mathbf{C}_e\mathbf{x}_e) \tag{5}$$

and the observer error is denoted by $\boldsymbol{\epsilon}_e = (\mathbf{x} - \mathbf{x}_e)$

3.2 Control law structure

In the considered on-orbit servicing applications, it is assumed that the spacecraft linear dynamics, $\mathbf{p}_0$, and the flexible dynamics, $\boldsymbol{\eta}$, are not measurable. In order to obtain the open-loop dynamics of the manipulator and reaction wheels, a re-writing effort of (2) is required to express the open-loop in function of measurable and estimated quantities. From (2), the manipulator and reaction wheels dynamics are given by:

$$\begin{aligned} &\mathbf{H}_q\ddot{\mathbf{q}} + \begin{bmatrix} \mathbf{0} & \mathbf{H}_{Lq}^T & \mathbf{H}_{\omega q}^T \end{bmatrix} \begin{bmatrix} \ddot{\boldsymbol{\eta}} \\ \ddot{\mathbf{p}}_0 \\ \dot{\boldsymbol{\omega}}_0 \end{bmatrix} + \mathbf{C}_q\dot{\mathbf{q}} \\ &+ \begin{bmatrix} \mathbf{0} & \mathbf{C}_{Lq}^T & \mathbf{C}_{\omega q}^T \end{bmatrix} \begin{bmatrix} \dot{\boldsymbol{\eta}} \\ \dot{\mathbf{p}}_0 \\ \boldsymbol{\omega}_0 \end{bmatrix} = \boldsymbol{\tau}_q \end{aligned} \tag{6}$$

As $\ddot{\mathbf{p}}_0$, $\ddot{\boldsymbol{\eta}}$ are not measurable and $\dot{\boldsymbol{\omega}}_0$ is not always properly measurable in on-orbit servicing applications, a re-writing effort is made by decomposing $\mathbf{D}^*(\mathbf{q}, \dot{\mathbf{q}}, \boldsymbol{\omega}_0, \dot{\mathbf{p}}_0)$ as $\mathbf{D}^*(\mathbf{q}, \dot{\mathbf{q}}, \boldsymbol{\omega}_0, \dot{\mathbf{p}}_0) = \left[\mathbf{D}^*_{\eta L\omega}(\mathbf{q}, \dot{\mathbf{q}}, \boldsymbol{\omega}_0, \dot{\mathbf{p}}_0)\ \mathbf{D}^*_q(\mathbf{q}, \dot{\mathbf{q}}, \boldsymbol{\omega}_0, \dot{\mathbf{p}}_0)\right]$ and injecting (3) in (6) to obtain the open-loop dynamics, detailed in appendix, as:

$$\begin{aligned} &\mathbf{M}^\diamond_q(\mathbf{q})\ddot{\mathbf{q}} + \mathbf{D}^\diamond_q(\mathbf{q}, \dot{\mathbf{q}}, \boldsymbol{\omega}_0, \dot{\mathbf{p}}_0)\dot{\mathbf{q}} \\ &+ \left[\mathbf{K}^\diamond(\mathbf{q})\ \mathbf{D}^\diamond_{\eta L\omega}(\mathbf{q}, \dot{\mathbf{q}}, \boldsymbol{\omega}_0, \dot{\mathbf{p}}_0)\right] \bar{\mathbf{C}}_e\mathbf{x} = \boldsymbol{\tau}_q \end{aligned} \tag{7}$$

where $\left[\eta^T \ \dot{\boldsymbol{\eta}}^T \ \dot{\mathbf{p}}_0^T \ \boldsymbol{\omega}_0^T\right]^T = \bar{\mathbf{C}}_e\mathbf{x}$

Decoupling actuators from each others allows to reduce the impact of the undesired vibrations and the drift of the spacecraft on the actuator control performances as well as improving the flexibility of their use to attenuate the intern disturbances as detailed in Kraïem et al. (2021). In order to decouple actuators, a Nonlinear Dynamic Inversion is proposed. In order to obtain the NDI, one can introduce the on-line measurement and estimation of the quantities $\mathbf{q}$, $\boldsymbol{\omega}_0$ and $\dot{\mathbf{p}}_0$ with the notations $\hat{\mathbf{q}}$, $\hat{\boldsymbol{\omega}}_0$ and $\dot{\mathbf{p}}_{0_e}$ and the inverse kinematics as $\hat{\mathbf{H}} = \mathbf{H}(\hat{\mathbf{q}})$ and $\hat{\mathbf{C}} = \mathbf{C}(\hat{\mathbf{q}}, \dot{\hat{\mathbf{q}}}, \hat{\boldsymbol{\omega}}_0, \dot{\mathbf{p}}_{0_e})$. From (7), nonlinear feedback linearization is now easily obtained (for a given dynamics $\mathbf{v}$) by posing the commanded torque:

$$\boldsymbol{\tau}_{q_c} = \hat{\mathbf{M}}^\diamond_q\mathbf{v} + \hat{\mathbf{D}}^\diamond_q\dot{\hat{\mathbf{q}}} + \left[\hat{\mathbf{K}}^\diamond\ \hat{\mathbf{D}}^\diamond_{\eta L\omega}\right] \bar{\mathbf{C}}_e\mathbf{x}_e \tag{8}$$

In order to consider errors from measurements when determining the inverse dynamics/kinematics, one can pose for any matrices $\hat{\mathbf{X}}$, $\hat{\mathbf{X}} = \mathbf{X} + \Delta\mathbf{X}$. However, for on-orbit servicing applications, one can consider that actuators are precise enough to assume that $\mathbf{q} = \hat{\mathbf{q}}$ and only consider measurement errors due to the spacecraft linear and angular dynamics measurements. One can then re-write (8) as:

$$\boldsymbol{\tau}_{q_c} = \mathbf{M}_q^{\diamond}\mathbf{v} + \hat{\mathbf{D}}_q^{\diamond}\dot{\mathbf{q}} + \begin{bmatrix}\mathbf{K}^{\diamond} & \hat{\mathbf{D}}_{\eta L\omega}^{\diamond}\end{bmatrix}\bar{\mathbf{C}}_e\mathbf{x}_e \tag{9}$$

3.3 System performances

In order to obtain controller and observer gain, we develop in this section the observer and controller dynamics.

Introducing the desired dynamics $\mathbf{v} = \ddot{\mathbf{q}}_d + \mathbf{K}\begin{bmatrix}\boldsymbol{\epsilon}_c \\ \dot{\boldsymbol{\epsilon}}_c\end{bmatrix}$, with $\mathbf{K}$ the controller gain and $\boldsymbol{\epsilon}_c = \mathbf{q}_d - \hat{\mathbf{q}}$, by injecting (9) in (7), the closed-loop is obtained as:

$$\begin{aligned}\mathbf{M}_q^{\diamond}\ddot{\mathbf{q}} + \mathbf{D}_q^{\diamond}\dot{\mathbf{q}} + \begin{bmatrix}\mathbf{K}^{\diamond} & \mathbf{D}_{\eta L\omega}^{\diamond}\end{bmatrix}\bar{\mathbf{C}}_e\mathbf{x} = \mathbf{M}_q^{\diamond}\mathbf{v} \\ + \hat{\mathbf{D}}_q^{\diamond}\dot{\mathbf{q}} + \begin{bmatrix}\mathbf{K}^{\diamond} & \hat{\mathbf{D}}_{\eta L\omega}^{\diamond}\end{bmatrix}\bar{\mathbf{C}}_e\mathbf{x}_e\end{aligned} \tag{10}$$

From (10), one can express the control error dynamics as:

$$\begin{aligned}\ddot{\boldsymbol{\epsilon}}_c = -\mathbf{K}\begin{bmatrix}\boldsymbol{\epsilon}_c \\ \dot{\boldsymbol{\epsilon}}_c\end{bmatrix} + \mathbf{M}_q^{\diamond^{-1}}\Delta\mathbf{D}_q^{\diamond}\dot{\mathbf{q}} + \mathbf{M}_q^{\diamond^{-1}}\begin{bmatrix}\mathbf{K}^{\diamond} & \mathbf{D}_{\eta L\omega}^{\diamond}\end{bmatrix}\bar{\mathbf{C}}_e\boldsymbol{\epsilon}_e \\ - \mathbf{M}_q^{\diamond^{-1}}\begin{bmatrix}\mathbf{0} & \Delta\mathbf{D}_{\eta L\omega}^{\diamond}\end{bmatrix}\bar{\mathbf{C}}_e\mathbf{x}_e\end{aligned} \tag{11}$$

To simplify (11), one can assume $\dot{\mathbf{q}}_e = \dot{\mathbf{q}}$ an re-write (11)

$$\begin{aligned}\ddot{\boldsymbol{\epsilon}}_c = -\mathbf{K}\begin{bmatrix}\boldsymbol{\epsilon}_c \\ \dot{\boldsymbol{\epsilon}}_c\end{bmatrix} + \mathbf{M}_q^{\diamond^{-1}}\begin{bmatrix}\mathbf{K}^{\diamond} & \mathbf{D}_{\eta L\omega}^{\diamond}\end{bmatrix}\bar{\mathbf{C}}_e\boldsymbol{\epsilon}_e \\ - \mathbf{M}_q^{\diamond^{-1}}\begin{bmatrix}\mathbf{0} & \Delta\mathbf{D}_{\eta L\omega}^{\diamond} & -\Delta\mathbf{D}_q^{\diamond}\end{bmatrix}\mathbf{x}_e\end{aligned} \tag{12}$$

Likewise, the observer error dynamics is given by:

$$\begin{aligned}\dot{\boldsymbol{\epsilon}}_e = \dot{\mathbf{x}} - \dot{\mathbf{x}}_e = \mathbf{A}_e\mathbf{x} + \mathbf{B}_e\ddot{\mathbf{q}} - \left(\hat{\mathbf{A}}_e\mathbf{x}_e + \mathbf{B}_e\mathbf{v} + \mathbf{L}\mathbf{C}_e\boldsymbol{\epsilon}_e\right) \\ = (\mathbf{A}_e - \mathbf{L}\mathbf{C}_e)\boldsymbol{\epsilon}_e - \Delta\mathbf{A}_e\mathbf{x}_e - \mathbf{B}_e\ddot{\boldsymbol{\epsilon}}_c - \mathbf{B}_e\mathbf{K}\begin{bmatrix}\boldsymbol{\epsilon}_c \\ \dot{\boldsymbol{\epsilon}}_c\end{bmatrix}\end{aligned} \tag{13}$$

The observer dynamics is function of the controller dynamics, by injecting (12) in (13), one can express the observer error dynamics in function of the observer gain $\mathbf{L}$:

$$\begin{aligned}\dot{\boldsymbol{\epsilon}}_e = \left(\mathbf{A}_e - \mathbf{B}_e\mathbf{M}_q^{\diamond^{-1}}\begin{bmatrix}\mathbf{K}^{\diamond} & \mathbf{D}_{\eta L\omega}^{\diamond}\end{bmatrix}\bar{\mathbf{C}}_e - \mathbf{L}\mathbf{C}_e\right)\boldsymbol{\epsilon}_e \\ - \left(\Delta\mathbf{A}_e - \mathbf{B}_e\mathbf{M}_q^{\diamond^{-1}}\begin{bmatrix}\mathbf{0} & \Delta\mathbf{D}_{\eta L\omega}^{\diamond} & -\Delta\mathbf{D}_q^{\diamond}\end{bmatrix}\right)\mathbf{x}_e\end{aligned} \tag{14}$$

One can note the dependency between both dynamics, which motivates a simultaneous synthesis to compute both controller and observer gains.

3.4 Simultaneous synthesis

Let's pose $\mathbf{z} = \begin{bmatrix}\boldsymbol{\epsilon}_c \\ \dot{\boldsymbol{\epsilon}}_c\end{bmatrix}$, $\mathbf{w} = \mathbf{x}_e$ and with (12) and (14) one can consider the system, detailed in appendix C:

$$\begin{cases}\dot{\mathbf{z}} = (\mathbf{A}_z + \mathbf{B}_z\mathbf{K})\,\mathbf{z} + \mathbf{B}_{\epsilon_z}\boldsymbol{\epsilon}_e + \mathbf{B}_{w_z}\mathbf{w} & \text{(15a)} \\ \dot{\boldsymbol{\epsilon}}_e = (\mathbf{A}_\epsilon - \mathbf{L}\mathbf{C}_e)\,\boldsymbol{\epsilon}_e + \mathbf{B}_{w_\epsilon}\mathbf{w} & \text{(15b)} \\ \boldsymbol{\epsilon}_c = \mathbf{C}_z\mathbf{z} & \text{(15c)}\end{cases}$$

Using the augmented state $\mathbf{X} = \begin{bmatrix}\mathbf{z}^T & \boldsymbol{\epsilon}_e^T\end{bmatrix}^T$, a compact version is obtained:

$$\begin{cases}\dot{\mathbf{X}} = \begin{bmatrix}\mathbf{A}_z + \mathbf{B}_z\mathbf{K} & \mathbf{B}_{\epsilon_z} \\ \mathbf{0} & \mathbf{A}_\epsilon - \mathbf{L}\mathbf{C}_e\end{bmatrix}\mathbf{X} + \begin{bmatrix}\mathbf{B}_{w_z} \\ \mathbf{B}_{w_\epsilon}\end{bmatrix}\mathbf{w} & \text{(16a)} \\ \quad = \mathbf{A}\mathbf{X} + \mathbf{B}\mathbf{w} \\ \boldsymbol{\epsilon}_c = [\mathbf{C}_z\ \mathbf{0}]\,\mathbf{X} = \mathbf{C}\mathbf{X} & \text{(16b)}\end{cases}$$

We assume that the estimation error verifies $\boldsymbol{\epsilon}_0^T\mathbf{E}\boldsymbol{\epsilon}_0 \leq 1$ for a given positive definite matrix $\mathbf{E}$, where $\boldsymbol{\epsilon}_0$ is the initial condition of the observer error. Likewise, $\mathbf{w}$ is bounded in the considered servicing scenario. The control and observer gains are obtained with the LMI resolution given in the following proposition.

Proposition: If there exist symmetric positive definite matrices $\mathbf{Q}_z$, $\mathbf{P}_\epsilon$ and matrices $\mathbf{W}_z$, $\mathbf{W}_\epsilon$ of appropriate dimensions such that for a given scalar $\gamma > 0$ the following LMI constraint holds:

$$\begin{bmatrix}\Omega & \begin{bmatrix}\mathbf{B}_{w_z} \\ \mathbf{P}_\epsilon\mathbf{B}_{w_\epsilon}\end{bmatrix} & \begin{bmatrix}\mathbf{Q}_z\mathbf{C}_z^T \\ \mathbf{0}\end{bmatrix} \\ * & -\gamma\mathbf{I} & \mathbf{0} \\ * & * & -\gamma\mathbf{I}\end{bmatrix} < 0 \tag{17}$$

where $\Omega = \begin{bmatrix}(\mathbf{A}_z\mathbf{Q}_z + \mathbf{B}_z\mathbf{W}_z)^{\mathbf{s}} & \mathbf{B}_{\epsilon_z} \\ * & (\mathbf{P}_\epsilon\mathbf{A}_\epsilon - \mathbf{W}_\epsilon\mathbf{C}_e)^{\mathbf{s}}\end{bmatrix}$

Then system (15) is quadratically stabilized with $\mathbf{K} = \mathbf{W}_z\mathbf{Q}_z^{-1}$ and $L = \mathbf{P}_\epsilon^{-1}\mathbf{W}_\epsilon$. Moreover, the outputs $\boldsymbol{\epsilon}_c$ verify:

$$\forall\ \mathbf{T} > 0, \int_0^{\mathbf{T}} \boldsymbol{\epsilon}_c(t)^T\boldsymbol{\epsilon}_c(t)dt < \gamma^2\int_0^{\mathbf{T}} \mathbf{w}(t)^T\mathbf{w}(t)dt \tag{18}$$

Proof: This is a straightforward adaptation of the LMI formulation of the bounded real lemma Boyd et al. (1994) using the following bloc diagonal Lyapunov function $\mathbf{V}(\mathbf{X}) = \mathbf{X}^T\begin{bmatrix}\mathbf{Q}_z^{-1} & \mathbf{0} \\ \mathbf{0} & \mathbf{P}_\epsilon\end{bmatrix}\mathbf{X}$ and standard change of variables to eliminate bilinear terms.

The state vector $\begin{bmatrix}\boldsymbol{\theta}_0^T & \mathbf{p}_0^T & \mathbf{q}^T & \boldsymbol{\eta}^T\end{bmatrix}^T$ and its derivatives are bounded for a given manipulator motion which thus bound matrices in (3) and (7). Thanks to the following lemma, to take into account bounded uncertainties that affect notably $\mathbf{B}_{\epsilon_z}$ and $\mathbf{B}_{w_z}$, relaxation term $\rho\mathbf{I}$ can be tuned such that:

$$\Omega = \begin{bmatrix}(\mathbf{A}_z\mathbf{Q}_z + \mathbf{B}_z\mathbf{W}_z)^{\mathbf{s}} + \rho\mathbf{I} & \mathbf{B}_{\epsilon_z} \\ * & (\mathbf{P}_\epsilon\mathbf{A}_\epsilon - \mathbf{W}_\epsilon\mathbf{C}_e)^{\mathbf{s}} + \rho\mathbf{I}\end{bmatrix}$$

Indeed, observing the following lemma, relaxation terms allow to deal with variations and uncertainties of the system during the space-robot motions.

Lemma:

$$\begin{bmatrix}\Psi_1 + \rho\mathbf{I} & \mathbf{B} \\ \mathbf{B}^T & \Psi_2 + \rho_2\mathbf{I}\end{bmatrix} < 0 \Rightarrow \begin{bmatrix}\Psi_1 & B + \Delta \\ \mathbf{B}^T + \Delta^T & \Psi_2\end{bmatrix} < 0$$
$$\forall\ \Delta \mid \Delta^T\Delta < \rho\mathbf{I}$$

Proof:

$$\begin{bmatrix} \Psi_1 & \mathbf{B}+\Delta \\ \mathbf{B}^T+\Delta^T & \Psi_2 \end{bmatrix} = \underbrace{\begin{bmatrix} \Psi_1+\rho\mathbf{I} & \mathbf{B} \\ \mathbf{B}^T & \Psi_2+\rho\mathbf{I} \end{bmatrix}}_{<0} + \underbrace{\begin{bmatrix} -\rho\mathbf{I} & \Delta \\ \Delta^T & -\rho\mathbf{I} \end{bmatrix}}_{<0} < 0 \iff \rho^2\mathbf{I} > \Delta^T\Delta$$

4. ILLUSTRATION OF THE PROPOSED METHOD

4.1 Study case

In order to illustrate our proposed method, the on-orbit deployment of the PULSAR telescope presented in Rognant et al. (2019a) is considered. The deployment is divided in different motions, in which either the manipulator moves a mirror tile or a bundle of tiles or is reaching to grab a tile.

For illustration purposes, one can consider a sequence in which a 44 kg mirror tile manipulated by the PULSAR's 8 DOF manipulator of 327 kg and 6 identical reaction wheels with an angular momentum at nominal speed of 0.75 $N.m.s$ to control base rotations. A total of 22 flexible modes are divided between the beams of the solar shields and the solar arrays. The total mass of the spacecraft is 6892 kg. For the considered deployment sequence, one can evaluate the bounded sets of matrices depending on the measurement errors of $\boldsymbol{\omega}_0$. An error of 10% corresponds to a variation of the norm of matrix $\mathbf{C}$ between $[-1.9;\ -1.7]$. Moreover, in the controller and observer synthesis, parameter ρ is obtained to deal with system variations in the sequence considered. The variations correspond to the impact of the observer error dynamics on the control dynamics. To obtain this parameter, one can evaluate the variations of $\mathbf{B}_{\epsilon_z}$ for the variations of the manipulator under the assumption that the base is maintained fixed (i.e. $\boldsymbol{\omega}_0 = 0$) and by constraining the manipulator joints velocities according to the reaction wheels capacity obtained with the kinetic moment conservation for the rigid spacecraft (see Wilde et al. (2018)). According to the lemma in section 3.4.3, the parameter ρ is obtained as 6.8.

4.2 Simulations results

The YALMIP toolbox (see Löfberg (2004)) with the MOSEK solver is used to solve the large dimension LMI of (17) while minimising the parameter λ. One can note that the system linearization allows to choose $\mathbf{Q}_z$ as a diagonal matrix in order to simplify the LMI resolution if necessary and impose different control dynamics for the reaction wheels and the manipulator joints.

To illustrate the proposed method efficiency, two cases are considered: 1) system variations and the actual measurement of $\boldsymbol{\omega}_0$ are taken into account and 2) system variations and additional bias to $\boldsymbol{\omega}_0$ measurements are taken into account. In both cases, the same manipulator path is considered and the reaction wheels velocities reference are such that the base remain fixed according to their capacities. As illustrated by Fig. 3 and 6, the use of the observer allows however the accuracy of the measurement of $\boldsymbol{\omega}_0$ to reduce the disturbances torques (i.e. $[\mathbf{K}^{\diamond}\ \mathbf{D}^{*}]\,\mathbf{x}_e$) on the manipulator control torques and by consequence allows to reduce the impact of base disturbances on the control performances. However, better the measurement of $\boldsymbol{\omega}_0$ is, better are the disturbance torque rejection. Likewise, in addition of stabilizing the system, the gains synthesis with the relaxation term ρ to maintain equivalent control performances of the manipulator as illustrated in Fig. 5 and 8. Moreover, for same reasons, the reaction wheels control performances remain similar in both cases as illustrated by Fig 4 and 7.

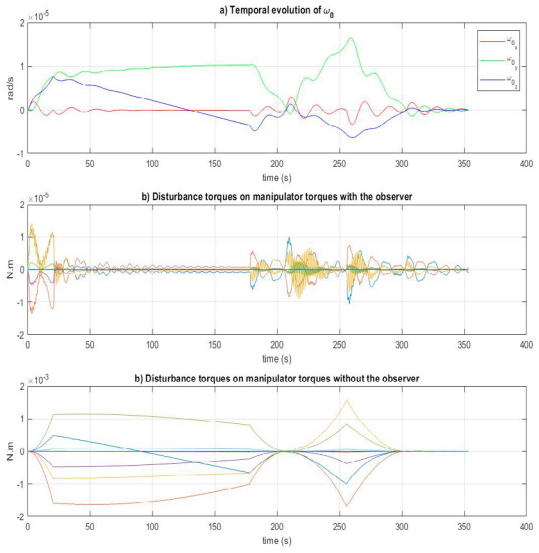

Fig. 3. Evolution of: a) $\boldsymbol{\omega}_0$; b) the disturbance torques on the manipulator control torques with the observer; c) the disturbance torques on the manipulator control torques without the observer; in case 1)

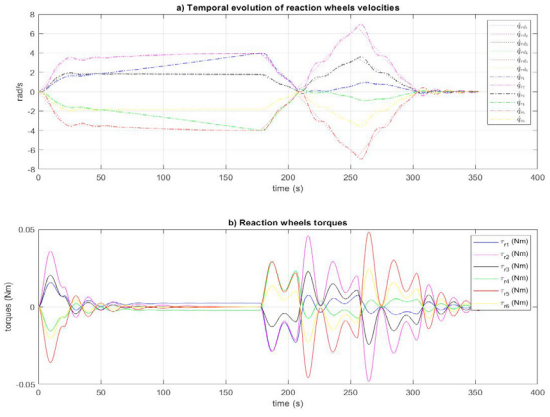

Fig. 4. Evolution of: a) $\dot{\mathbf{q}}_r$ and $\dot{\mathbf{q}}_{r_d}$; b) $\boldsymbol{\tau}_r$; in case 1)

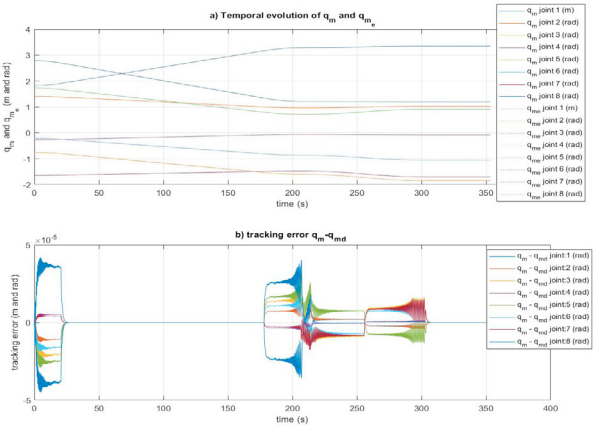

Fig. 5. Evolution of: a) $\mathbf{q}_m$ and $\mathbf{q}_{m_d}$; b) $\boldsymbol{\epsilon}_{c_m}$; in case 1)

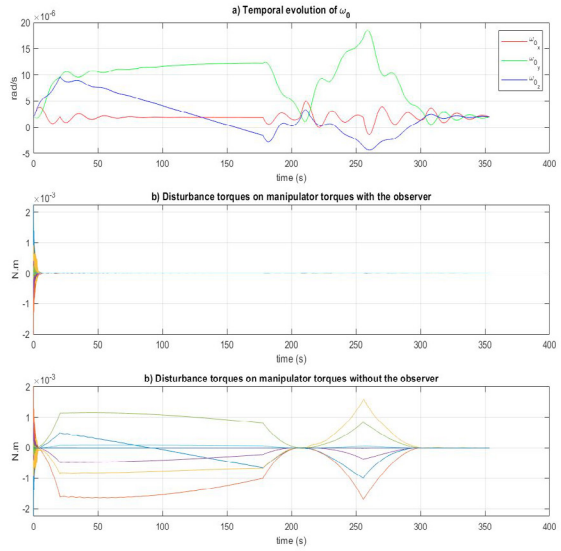

Fig. 6. Evolution of: a) $\boldsymbol{\omega}_0$; b) the disturbance torques on the manipulator control torques with the observer; c) the disturbance torques on the manipulator control torques without the observer; in case 2)

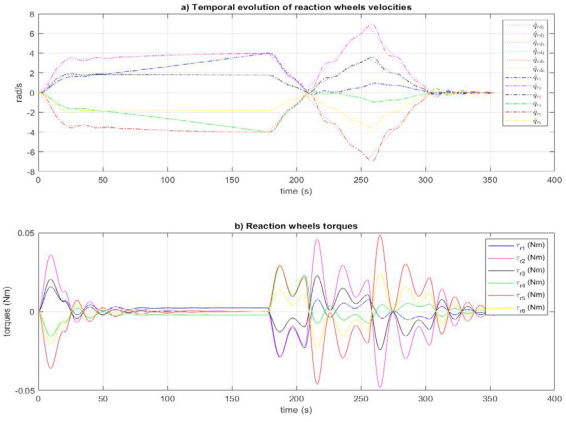

Fig. 7. Evolution of: a) $\dot{\mathbf{q}}_r$ and $\dot{\mathbf{q}}_{r_d}$; b) $\boldsymbol{\tau}_r$; in case 2)

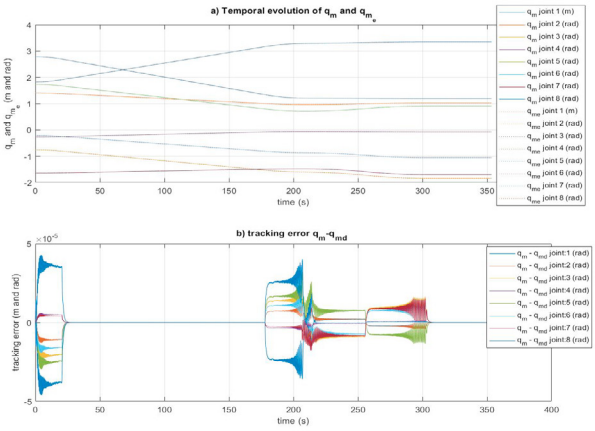

Fig. 8. Evolution of: a) $\mathbf{q}_m$ and $\mathbf{q}_{m_d}$; b) $\boldsymbol{\epsilon}_{c_m}$; in case 2)

5. CONCLUSION

After presenting the interest of a common base and manipulator control of a rotation free-floating space manipulator in Rognant et al. (2019b), and illustrating the feasibility and benefits of including the estimations of system disturbances in the NDI in Kraïem et al. (2021), an extension of our work is proposed in this paper. An adaptation of the observer with hypothesis based on available measurements in most of OOS applications is developed. The derivation of the rotation free-floating spacecraft dynamics allows to include the linear dynamics of the spacecraft and the appendages vibrations in the NDI and improve control performances. The observer and gain synthesis includes OOS usual measurement errors and system variations during the considered deployment sequence and is dependent on a pre-planned manipulator trajectory. Simulations on an actual deployment scenario allows to illustrate the efficiency and feasibility of the method. Future works should focus on a gain synthesis for the complete deployment scenario which remain challenging as significant inertia variations are considered.

ACKNOWLEDGEMENTS

The PULSAR project is funded under the European Commission's Horizon 2020 Space Strategic Research Cluster Operational Grants, grant number 821858. The authors would like to thank M. Aurélien Cuffolo, from Thales AleniaSpace in France, partner in the PULSAR consortium, for providing inputs on mission analysis, spacecraft sizing and AOCS models.

REFERENCES

Alazard, D. et al. (2008). Linear dynamic modeling of spacecraft with various flexible appendages and on-board angular momentums.

Boyd, S. et al. (1994). *Linear matrix inequalities in system and control theory.* SIAM.

Flores-Abad et al. (2014). A review of space robotics technologies for on-orbit servicing. *Progress in Aerospace Sciences*, 68.

Giordano, A.M. et al. (2018). Workspace fixation for free-floating space robot operations. In *2018 IEEE*

International Conference on Robotics and Automation (ICRA), 889–896. IEEE.
Giordano, A.M., Ott, C., and Albu-Schäffer, A. (2019). Coordinated control of spacecraft's attitude and end-effector for space robots. *IEEE Robotics and Automation Letters*, 4(2), 2108–2115.
Kraïem, S. et al. (2021). Control of rotation-floating space robots with flexible appendages for on-orbit servicing. In *European Control Conference*.
Li, K. et al. (2019a). Assembly dynamics of a large space modular satellite antenna. *Mechanism and Machine Theory*, 142, 103601.
Li, W.J. et al. (2019b). On-orbit service (oos) of spacecraft: A review of engineering developments. *Progress in Aerospace Sciences*, 108, 32–120.
Li, Z. et al. (2013). Motion planning and coordination control of space robot using methods of calculated momentum. In *2013 IEEE International Conference on Robotics and Biomimetics (ROBIO)*. IEEE.
Löfberg, J. (2004). Yalmip : A toolbox for modeling and optimization in matlab. In *In Proceedings of the CACSD Conference*.
Lu, J. and Yang, H. (2020). Trajectory planning of satellite base attitude disturbance optimization for space robot. In *2020 3rd International Conference on Control and Robots (ICCR)*, 85–89. IEEE.
Lu, Y., Huang, Z., Zhang, W., Wen, H., and Jin, D. (2020). Experimental investigation on automated assembly of space structure from cooperative modular components. *Acta Astronautica*, 171, 378–387.
Meng, D. et al. (2018). Vibration suppression control of free-floating space robots with flexible appendages for autonomous target capturing. *Acta Astronautica*, 151, 904–918.
Pisculli, A. et al. (2015). A minimum state multibody/fem approach for modeling flexible orbiting space systems. *Acta Astronautica*.
Qiao, J. et al. (2019). High-precision attitude tracking control of space manipulator system under multiple disturbances. *IEEE Transactions on Systems, Man, and Cybernetics: Systems*.
Rognant, M. et al. (2019a). Autonomous assembly of large structures in space: a technology review. In *8th European Conference for Aeronautics and Aerospace Sciences (EUCASS)*.
Rognant, M. et al. (2019b). Kinematic indices of rotation-floating space robots for on-orbit servicing. In *IFToMM World Congress on Mechanism and Machine Science*, 3107–3116. Springer.
Rybus, T. et al. (2017). Control system for free-floating space manipulator based on nonlinear model predictive control (nmpc). *Journal of Intelligent & Robotic Systems*, 85(3-4), 491–509.
Seddaoui, A. and Saaj, C.M. (2019). Combined nonlinear h controller for a controlled-floating space robot. *Journal of Guidance, Control, and Dynamics*, 42(8), 1878–1885.
Song, Y. et al. (2019). Review on on-orbit assembly of large space telescopes. In *AOPC 2019: Space Optics, Telescopes, and Instrumentation*. International Society for Optics and Photonics.
Virgili-Llop, J. et al. (no date). SPART: an open-source modeling and control toolkit for mobile-base robotic multibody systems with kinematic tree topologies. `https://github.com/NPS-SRL/SPART`.
Wilde, M. et al. (2018). Equations of motion of free-floating spacecraft-manipulator systems: An engineer's tutorial. *Frontiers in Robotics and AI*, 5, 41.
Wu, Y. et al. (2018). Attitude control for on-orbit servicing spacecraft using hybrid actuator. *Advances in Space Research*, 61(6).

Appendix A. DETAIL OF (3)

To alleviate further notations, one can pose: $\mathbf{H}_{\eta L\omega}^{-1} = \begin{bmatrix} \mathbf{H}_\eta & \mathbf{H}_{L\eta}^T & \mathbf{H}_{\omega\eta}^T \\ \mathbf{H}_{L\eta} & \mathbf{H}_L & \mathbf{H}_{L\omega} \\ \mathbf{H}_{\omega\eta} & \mathbf{H}_{\omega L} & \mathbf{H}_\omega \end{bmatrix}$

$$\begin{cases} \mathbf{M}^* = \mathbf{H}_{\eta L\omega}^{-1} \begin{bmatrix} \mathbf{0} \\ \mathbf{H}_{Lq} \\ \mathbf{H}_{\omega q} \end{bmatrix} \\ \mathbf{D}^* = \mathbf{H}_{\eta L\omega}^{-1} \begin{bmatrix} \mathbf{C}_\eta & \mathbf{C}_{L\eta}^T & \mathbf{C}_{\omega\eta}^T & \mathbf{0} \\ \mathbf{C}_{L\eta} & \mathbf{C}_L & \mathbf{C}_{L\omega} & \mathbf{C}_{Lq} \\ \mathbf{C}_{\omega\eta} & \mathbf{C}_{\omega L} & \mathbf{C}_\omega & \mathbf{C}_{\omega q} \end{bmatrix} \\ \mathbf{K}^* = \mathbf{H}_{\eta L\omega}^{-1} \begin{bmatrix} \mathbf{K}_\eta \\ \mathbf{0} \\ \mathbf{0} \end{bmatrix} \end{cases}$$

Appendix B. DETAIL OF (7)

$$\begin{cases} \mathbf{M}_q^\diamond = \mathbf{H}_q - \begin{bmatrix} \mathbf{0} & \mathbf{H}_{Lq}^T & \mathbf{H}_{\omega q}^T \end{bmatrix} \mathbf{M}^* \\ \mathbf{D}_q^\diamond = \mathbf{C}_q - \begin{bmatrix} \mathbf{0} & \mathbf{H}_{Lq}^T & \mathbf{H}_{\omega q}^T \end{bmatrix} \mathbf{D}_q^* \\ \mathbf{K}^\diamond = - \begin{bmatrix} \mathbf{0} & \mathbf{H}_{Lq}^T & \mathbf{H}_{\omega q}^T \end{bmatrix} \mathbf{K}^* \\ \mathbf{D}_{\eta L\omega}^\diamond = \begin{bmatrix} \mathbf{0} & \mathbf{C}_{Lq}^T & \mathbf{C}_{\omega q}^T \end{bmatrix} - \begin{bmatrix} \mathbf{0} & \mathbf{H}_{Lq}^T & \mathbf{H}_{\omega q}^T \end{bmatrix} \mathbf{D}_{\eta L\omega}^* \end{cases}$$

Appendix C. DETAIL OF (15)

With (12) and (14), one can detail matrices in (15) as:

$$\mathbf{A}_z = \begin{bmatrix} \mathbf{0} & \mathbf{I} \\ \mathbf{0} & \mathbf{0} \end{bmatrix} \tag{C.1a}$$

$$\mathbf{B}_z = \begin{bmatrix} \mathbf{0} \\ -\mathbf{I} \end{bmatrix} \tag{C.1b}$$

$$\mathbf{B}_{\epsilon_z} = \begin{bmatrix} \mathbf{0} \\ \mathbf{M}_q^{\diamond^{-1}} \begin{bmatrix} \mathbf{K}^\diamond & \mathbf{D}_{\eta L\omega}^\diamond \end{bmatrix} \bar{\mathbf{C}}_e \end{bmatrix} \tag{C.1c}$$

$$\mathbf{B}_{w_z} = \begin{bmatrix} \mathbf{0} \\ -\mathbf{M}_q^{\diamond^{-1}} \begin{bmatrix} \mathbf{0} & \Delta\mathbf{D}_{\eta L\omega}^\diamond & \Delta\mathbf{D}_q^\diamond \end{bmatrix} \end{bmatrix} \tag{C.1d}$$

$$\mathbf{A}_\epsilon = \mathbf{A}_e - \mathbf{B}_e \mathbf{M}_q^{\diamond^{-1}} \begin{bmatrix} \mathbf{K}^\diamond & \mathbf{D}_{\eta L\omega}^\diamond \end{bmatrix} \bar{\mathbf{C}}_e \tag{C.1e}$$

$$\mathbf{B}_{w_\epsilon} = - \left(\Delta\mathbf{A}_e - \mathbf{B}_e \mathbf{M}_q^{\diamond^{-1}} \begin{bmatrix} \mathbf{0} & \Delta\mathbf{D}_{\eta L\omega}^\diamond & -\mathbf{D}_q^\diamond \end{bmatrix} \right) \tag{C.1f}$$

$$\mathbf{C}_z = \begin{bmatrix} \mathbf{I} & \mathbf{0} \end{bmatrix} \tag{C.1g}$$